

Global Bayesian Analysis of new physics in $b \rightarrow s\mu\mu$ transitions after Moriond-2019

Dinesh Kumar, Kamila Kowalska and Enrico Maria Sessolo
National Centre for Nuclear Research, Pasteura 7, 02-093 Warsaw, Poland

The recent measurement of R_K at LHCb continues to support the hint of violation of lepton flavor universality. We perform a global fit for new physics in semileptonic $b \rightarrow s$ transitions using all the relevant data with a Bayesian analysis technique. We include new measurements of R_K at LHCb and new determinations of R_{K^*} and $R_{K^{*+}}$ at Belle. We perform the scan for various NP scenarios and infer the 68% and 95.4% credibility regions of the marginalized posterior probability density for all scenarios. We also compare the models in pairs by calculating the Bayes factor given a common data set. A few well-known BSM models are analyzed that can provide a high energy framework for the EFT analysis. These include the exchange of a heavy Z' boson in models with heavy vector-like fermions and a scalar field, and a model with scalar leptoquarks. We provide predictions for the BSM couplings and expected mass values.

I. INTRODUCTION

The rare B decays are strongly suppressed in Standard Model (SM) due to CKM and by helicity. These decays can be useful for testing the New Physics (NP) beyond the SM (BSM). However, the lepton universality observables $R_{K^{(*)}}$ are very useful for testing the NP as the parameteric uncertainties cancel out at high precision in these ratios. Any small deviation from SM in these measurements will result to violation of lepton flavor universality (LFUV), which is a BSM phenomena.

Recently LHCb updated the measurement of R_K at Moriond-2019[1] and Belle also presented the result for R_{K^*} in B^0 -decays alongwith the counterpart $R_{K^{*+}}$ in B^+ -decays[2]. These updated results have been included in several global fits[3–6].

In this proceedings, we present our results which are reported in detail in ref [7]. We presented the global fit results of Bayesian analysis of the implication of new physics in semileptonic $b \rightarrow s$ transitions in model independent approach. We further analyzed a few well-known BSM models and provide the predictions for the BSM couplings and expected mass values.

II. FIT METHODOLOGY

We use the Bayesian approach to constrain the region of NP parameter space which can give a good fit to the data. In this approach, for a theory described by some parameters m , experimental observables $\xi(m)$ can be compared with data d and a pdf $p(m|d)$, of the model parameters m , can be calculated through Bayes' Theorem. This reads

$$p(m|d) = \frac{p(d|\xi(m))\pi(m)}{p(d)}, \quad (1)$$

where the likelihood $p(d|\xi(m)) \equiv \mathcal{L}(m)$ gives the probability density for obtaining d from a measurement of ξ given a specific value of m , and the prior $\pi(m)$

parametrizes assumptions about the theory prior to performing the measurement.

We define the likelihood function for the set m of input parameters

$$\mathcal{L}(m) = \exp \left\{ -\frac{1}{2} \left[\mathcal{O}_{\text{th}}(m) - \mathcal{O}_{\text{exp}} \right]^T (c^{\text{exp}} + c^{\text{th}})^{-1} \left[\mathcal{O}_{\text{th}}(m) - \mathcal{O}_{\text{exp}} \right] \right\}, \quad (2)$$

where \mathcal{O}_{th} and \mathcal{O}_{exp} are theoretical predictions and the experimental measurements observables, respectively. We have taken into account the available experimental correlation which is encoded in the matrix \mathcal{C}^{exp} . The V_{cb} element of the CKM matrix is treated as a real nuisance parameter. We scan it together with the models' input parameters, following a Gaussian distribution around its central Particle Data Group (PDG) value, and adopting PDG uncertainties. We always scan NP wilson coefficient from -3 to 3 .

III. RESULTS

The effective Hamiltonian for the $b \rightarrow sll$ transition can be written as:

$$\mathcal{H}_{\text{eff}} = -\frac{4G_F}{\sqrt{2}} V_{tb} V_{ts}^* \frac{e^2}{16\pi^2} \sum_{i,l} (C_i^l O_i^l + C_i'^l O_i'^l) + \text{H.c.}, \quad (3)$$

In this study, we assume the presence of NP in the following semi-leptonic operators:

$$O_9^{(l)} = (\bar{s}_{L(R)} \gamma^\mu b_{L(R)}) (\bar{l} \gamma_\mu l) \quad (4)$$

$$O_{10}^{(l)} = (\bar{s}_{L(R)} \gamma^\mu b_{L(R)}) (\bar{l} \gamma_\mu \gamma_5 l) \quad (5)$$

where the lepton l can be an electron or a muon. The full list of observables included in the fit can be found in ref. [7].

A. Model Independent Analysis

We present the posterior pdf of single non-zero NP wilson coefficient C_9^μ (left panel of figure 1) and

$C_9^\mu = -C_{10}^\mu$ (right panel of figure 1) marginalized over the nuisance parameter. The red and orange color represent the 1σ and 2σ credible regions, respectively. The gray dashed line shows the posterior pdf corresponding to the data pre-LHCb Run 2.

In the left panel of Fig.2, the posterior pdf for the

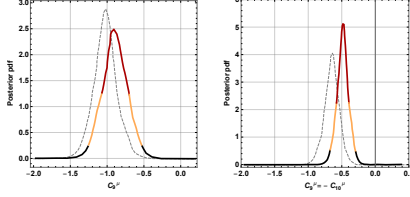


FIG. 1: (a) Posterior pdf for C_9^μ (left) and $C_9^\mu = -C_{10}^\mu$ (right).

scan in the input parameter (C_9^μ , C_{10}^μ) is presented. The red star marks the position of the best-fit point. The gray solid (dashed) line shows the 1σ (2σ) credible region of the pdf corresponding to the data pre-LHCb Run 2. The associated best-fit point is also shown in gray. The new measurement of R_K , which is slightly higher than the previous measurement, brings the 2σ region closer to the axes origin. In this case, in fact, one expects $R_K \approx R_{K^*}$ and a tension between the measurements of R_K and R_{K^*} arises as the posterior pdf becomes narrower. In the right panel of Fig.2, the posterior pdf for the scan in the input parameter C_9^μ , $C_9^{\prime\mu}$ is presented.

We performed a scan with 4 NP parameters C_9^μ ,

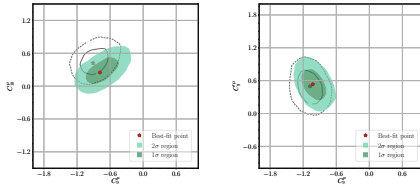


FIG. 2: Posterior pdf for (C_9^μ, C_{10}^μ) (left) and $(C_9^\mu, C_9^{\prime\mu})$ (right).

C_{10}^μ , $C_9^{\prime\mu}$, $C_{10}^{\prime\mu}$ and make the comparison between the marginalized pdf in the (C_9^μ, C_{10}^μ) plane for the scan with 2 input NP parameters, and the one with 4 NP parameters which is shown in the left of Figure 3. The large negative values of C_9^μ are favored by the data with 4 parameters. In the middle of Figure 3, we show a comparison between the marginalized pdf in the $(C_9^\mu, C_9^{\prime\mu})$. It can be seen that ample region of $C_9^{\prime\mu} \leq 0$ is allowed due to the introduction of $C_{10}^{\prime\mu}$. The explicit correlation between the $C_9^{\prime\mu}$ and $C_{10}^{\prime\mu}$ in the right of Figure 3 in case of scan with 4 parameters.

In upper left panel of Figure 4, we show the 1σ (dark) and 2σ (light) credible regions of the posterior pdf for the scan in the input parameter C_9^μ , C_{10}^μ , com-

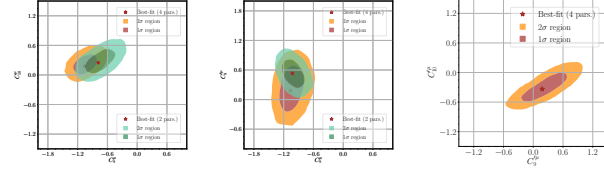


FIG. 3: Comparison of posterior pdf in 2 parameters and 4 parameters scan. The explicit correlation for $C_9^{\prime\mu}$ and $C_{10}^{\prime\mu}$ is also shown (with 4 parameter scan)

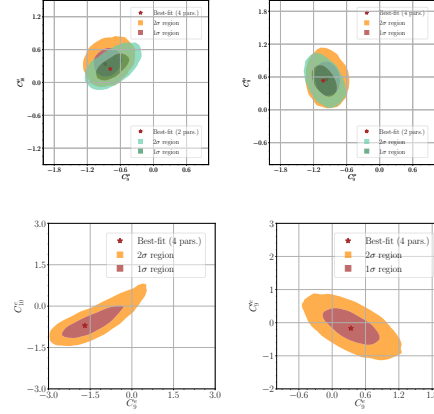


FIG. 4: Comparison of posterior pdf in 2 parameters and 4 parameters scan with NP in electron sector. The explicit correlation for only electron sector WC's in 4 parameters scan.

pared with the marginalized 2-dimensional regions in the same parameters for the scan with C_9^μ , C_{10}^μ , C_9^e , C_{10}^e all floating, which are shown in brown (1σ) and orange (2σ). A similar comparison of the posterior pdf for the scan in C_9^μ , $C_9^{\prime\mu}$ and the one with C_9^μ , $C_9^{\prime\mu}$, C_9^e , $C_9^{\prime e}$ all floating in the upper right panel of Figure 4. In the lower panel of Figure 4, a marginalized pdf for electron sector Wilson coefficients are presented which is consistent with zero at 2σ . This suggests that NP with only muon sector can easily explain the present data.

In Figure 5, we present the marginalized pdf for 8 parameter scan in most relevant planes (C_9^μ, C_{10}^μ) and $(C_9^\mu, C_9^{\prime\mu})$ in the left and right panel. These marginal pdf are compared with 2 parameter scan and we find that these figures are almost same as Figure 3 which is expected as the NP wilson coefficients in the electron sector have limited impact on the data.

We use Jeffrey's scale to quickly assess the Bayes factor, which will point to which model is favored by the data. We find that models with scenario $(C_9^\mu, C_9^{\prime\mu})$ and C_9^μ , C_{10}^μ , $C_9^{\prime\mu}$, $C_{10}^{\prime\mu}$ are slightly favored by the data. We have summarized all 8 scans in Table I. In order to make contact with frequentist approach, the best fit values of wilson coefficients with R_K and R_{K^*} at best fit points is presented in Table II.

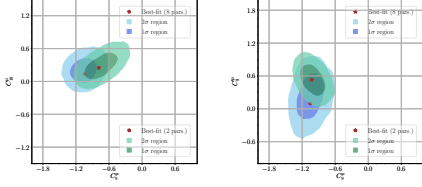


FIG. 5: Comparison of posterior pdf in 2 parameters versus 8 parameters scan.

Input parameters	$\ln Z$	Pull	χ^2_{TOT}	$\chi^2_{\text{TOT}}/d.o.f$	χ^2_μ	χ^2_e	$\chi^2_{R_K}$	$\chi^2_{R_{K^*}}$
SM	88.5	—	174.7	1.29	145.7	6.5	8.1	12.0
	88.3	—	174.4	1.24	145.7	6.5	6.2	13.6
C_9^μ	75.8	5.0 σ	145.6	1.09	132.5	6.7	0.2	6.0
	77.3	4.7 σ	148.4	1.06	132.2	6.6	0.3	8.9
$C_9^\mu = -C_{10}^\mu$	74.4	5.3 σ	142.4	1.06	132.4	6.8	0.2	3.0
	77.5	4.8 σ	148.2	1.06	133.2	6.7	1.2	7.0
C_9^μ, C_{10}^μ	74.5	5.3 σ	140.1	1.05	129.8	6.8	0.2	3.4
	77.6	4.7 σ	146.1	1.05	130.3	6.7	1.5	7.6
$C_9^\mu, C_9^{\prime\mu}$	75.1	5.2 σ	141.1	1.06	128.1	6.7	2.0	4.1
	75.8	5.0 σ	142.3	1.02	127.6	6.7	0.5	7.3
$C_9^\mu, C_{10}^\mu, C_9^{\prime\mu}, C_{10}^{\prime\mu}$	74.0	5.4 σ	133.3	1.02	123.5	6.8	0.6	2.4
	76.0	5.1 σ	136.8	1.00	123.2	6.8	0.0	6.8
$C_9^\mu, C_{10}^\mu, C_9^e, C_{10}^e$	75.6	4.9 σ	138.8	1.06	129.7	6.9	0.0	2.1
	78.0	4.5 σ	142.7	1.04	129.8	7.1	0.1	5.8
$C_9^\mu, C_9^e, C_9^{\prime\mu}, C_9^{\prime e}$	75.8	4.9 σ	138.5	1.06	127.5	7.8	0.5	2.4
	77.7	4.6 σ	141.6	1.03	127.2	7.0	0.2	6.7
$(C_9^\mu, C_{10}^\mu, C_9^{\prime\mu}, C_{10}^{\prime\mu})$	76.2	4.7 σ	132.4	1.04	123.3	6.7	0.3	2.1
$(C_9^e, C_{10}^e, C_9^{\prime e}, C_{10}^{\prime e})$	78.3	4.4 σ	135.4	1.02	123.3	6.6	0.2	5.4

TABLE I: Evidence, pull from the SM, and chi-squared statistics for the best-fit points of the considered scenarios. Second row in each block correspond to the new data, while the first ones show the previous determinations.

IV. MODEL DEPENDENT ANALYSIS

A. Heavy Z'

The most generic Lagrangian, parametrizing LFUV couplings of Z' to the b - s current and the muons reads

$$\mathcal{L} \supset Z'_\alpha (\Delta_L^{sb} \bar{s}_L \gamma^\alpha b_L + \Delta_R^{sb} \bar{s}_R \gamma^\alpha b_R + \text{H.c.}) + Z'_\alpha (\Delta_L^{\mu\mu} \bar{\mu}_L \gamma^\alpha \mu_L + \Delta_R^{\mu\mu} \bar{\mu}_R \gamma^\alpha \mu_R). \quad (6)$$

The relevant Wilson coefficients are then given by

$$C_{9,\text{NP}}^{(\prime)\mu} = -2 \frac{\Delta_L^{sb} \Delta_R^{\mu\mu}}{V_{tb} V_{ts}^*} \left(\frac{\Lambda_v}{m_{Z'}} \right)^2, \quad C_{10,\text{NP}}^{(\prime)\mu} = -2 \frac{\Delta_R^{sb} \Delta_L^{\mu\mu}}{V_{tb} V_{ts}^*} \left(\frac{\Lambda_v}{m_{Z'}} \right)^2, \quad (7)$$

where $\Delta_9^{\mu\mu} \equiv (\Delta_R^{\mu\mu} + \Delta_L^{\mu\mu})/2$, $\Delta_{10}^{\mu\mu} \equiv (\Delta_R^{\mu\mu} - \Delta_L^{\mu\mu})/2$, $m_{Z'}$ is the mass of the Z' boson, and $\Lambda_v = \left(\frac{\pi}{\sqrt{2} G_F \alpha_{\text{em}}} \right)^{1/2} \approx 4.94 \text{ TeV}$, is the typical effective scale of the new physics.

The coupling of heavy Z' to the gauge eigenstates must be flavor-conserving if it is the gauge boson of a new $U(1)_X$ gauge group and an additional structure

Input parameters	C_9^μ	C_{10}^μ	$C_9^{\prime\mu}$	$C_{10}^{\prime\mu}$	C_9^e	C_{10}^e	$C_9^{\prime e}$	$C_{10}^{\prime e}$
C_9^μ	-1.02	0	0	0	0	0	0	0
	-0.90	0	0	0	0	0	0	0
$C_9^\mu = -C_{10}^\mu$	-0.64	0.64	0	0	0	0	0	0
	-0.48	0.48	0	0	0	0	0	0
C_9^μ, C_{10}^μ	-0.91	0.42	0	0	0	0	0	0
	-0.78	0.25	0	0	0	0	0	0
$C_9^\mu, C_9^{\prime\mu}$	-1.08	0	0.49	0	0	0	0	0
	-1.03	0	0.53	0	0	0	0	0
$C_9^\mu, C_{10}^\mu, C_9^{\prime\mu}, C_{10}^{\prime\mu}$	-1.14	0.28	0.21	-0.31	0	0	0	0
	-1.06	0.18	0.18	-0.34	0	0	0	0
$C_9^\mu, C_{10}^\mu, C_9^e, C_{10}^e$	-0.92	0.40	0	0	-1.50	-0.90	0	0
	-0.88	0.34	0	0	-1.69	-0.71	0	0
$C_9^\mu, C_9^e, C_9^{\prime\mu}, C_9^{\prime e}$	-1.02	0	0.54	0	0.58	0	-0.17	0
	-0.97	0	0.55	0	0.34	0	-0.17	0
$(C_9^\mu, C_{10}^\mu, C_9^{\prime\mu}, C_{10}^{\prime\mu})$	-1.10	0.21	0.21	-0.30	-0.80	-0.63	-0.73	-0.57
$(C_9^e, C_{10}^e, C_9^{\prime e}, C_{10}^{\prime e})$	-1.05	0.13	0.10	-0.38	-2.18	-0.07	-2.73	-1.34

TABLE II: Wilson coefficients at the best-fit points, as well as the values there of R_K and R_{K^*} . Second row in each correspond to the new data, while the first ones show the previous determinations.

is required to generate Δ_L^{sb} and Δ_R^{sb} . Thus, in this work we also consider the impact of the new LHCb and Belle data on the masses and couplings of a few simplified but UV complete models.

Model 1. We consider a $U(1)_X$ model that has proven to be quite popular is the traditional $X = L_\mu - L_\tau$ model. Besides Z' , we also add to the SM a scalar singlet field S to spontaneously break the $U(1)_X$ symmetry and VL quark pairs Q, Q' and D, D' to create the flavor-changing couplings $\Delta_{L,R}^{bs}$ [9, 10].

Model 2. Another realization of the $L_\mu - L_\tau$ model we consider is an extension of the SM characterized by one pair of VL quark doublets Q, Q' , to generate the flavor-violating coupling of the Z' in the quark sector, Δ_L^{bs} , and one pair of VL $U(1)_X$ neutral leptons E, E' , which have to be $SU(2)$ singlets[11, 12].

Model 3. We finally consider an alternative to the $L_\mu - L_\tau$ model, obtained if one charges the VL leptons under the $U(1)_X$ symmetry, and leaves the SM leptons uncharged[13].

The gauge quantum numbers of the additional fermions and the contribution to the NP wilson coefficients in these models can be read from ref.[7]

We present the marginalized 2-dimensional posterior

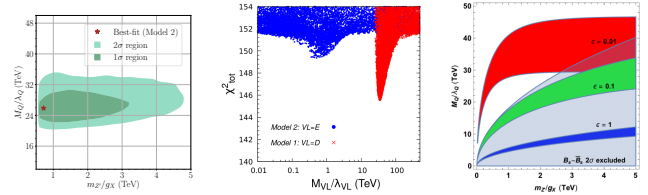


FIG. 6: Scan results for various models.

pdf in the $(m_{Z'}/g_X, M_Q/\lambda_Q)$ plane in Model 2 in left

of Figure 6. The VL mass range lies around a 20–30 TeV scale for a coupling λ_Q of order unity whereas the $m_{Z'}/g_X$ mass is limited to values below 5 TeV, as a result of the B_s mixing constraint. We find from middle of Figure 6 that in both Model 1 and Model 2, the second VL mass is unbounded from above at the 2σ level. This is a consequence of the fact that $C_{9,\text{NP}}^\mu$ in Model 1 and, especially $C_{10,\text{NP}}^\mu$ in Model 2, are consistent with zero at the 2σ level.

The 2σ regions of the 1-dimensional fit read

$$C_9^\mu = -C_{10}^\mu \in (-0.68, -0.29). \quad (8)$$

We apply this bound with B_s -mixing and show the favored 2σ region with different value of the hierarchical parameter ϵ , defined as $M_L/\lambda_{L,2} = \epsilon M_Q/\lambda_Q$ in right of Figure 6.

B. Leptoquark

Leptoquarks are considered potential candidate to explain the present flavor physics data. We consider a scalar leptoquark S_3 which Lagrangian acquires a Yukawa term

$$\mathcal{L} \supset Y_{ij} Q_i^T (i\sigma_2) S_3 L_j + \text{H.c.}, \quad (9)$$

The tree level contribution is

$$C_9^\mu = -C_{10}^\mu = \frac{\pi v^2}{V_{tb} V_{ts}^* \alpha_{\text{em}}} \frac{\hat{Y}_{b\mu} \hat{Y}_{s\mu}^*}{m_{S_3}^2}. \quad (10)$$

The constraint from the 1-dimensional EFT at 2σ is given in 8. This leads to

$$0.4 \times 10^{-3} \left(\frac{m_{S_3}}{\text{TeV}} \right)^2 \leq \hat{Y}_{b\mu} \hat{Y}_{s\mu}^* \leq 1.1 \times 10^{-3} \left(\frac{m_{S_3}}{\text{TeV}} \right)^2. \quad (11)$$

The most dangerous constraint is possibly given by $B \rightarrow K^{(*)} \nu \bar{\nu}$ decay. We get the limit

$$\Re(\hat{Y}_{b\mu} \hat{Y}_{s\mu}^*) \lesssim 2.2 \times 10^{-2} \left(\frac{m_{S_3}}{\text{TeV}} \right)^2, \quad (12)$$

which does not constrain the parameter space emerging in Eq. (11).

Acknowledgments

KK and DK are supported in part by the National Science Centre (Poland) under the research Grant No. 2017/26/E/ST2/00470. EMS is supported in part by the National Science Centre (Poland) under the research Grant No. 2017/26/D/ST2/00490. The use of the CIS computer cluster at the National Centre for Nuclear Research in Warsaw is gratefully acknowledged.

-
- [1] R. Aaij *et al.* [LHCb Collaboration], Phys. Rev. Lett. **122**, no. 19, 191801 (2019) doi:10.1103/PhysRevLett.122.191801 [arXiv:1903.09252 [hep-ex]].
 - [2] A. Abdesselam *et al.* [Belle Collaboration], arXiv:1904.02440 [hep-ex].
 - [3] M. Alguer, B. Capdevila, A. Crivellin, S. Descotes-Genon, P. Masjuan, J. Matias and J. Virto, arXiv:1903.09578 [hep-ph].
 - [4] A. K. Alok, A. Dighe, S. Gangal and D. Kumar arXiv:1903.09617 [hep-ph].
 - [5] M. Ciuchini, A. M. Coutinho, M. Fedele, E. Franco, A. Paul, L. Silvestrini and M. Valli, arXiv:1903.09632 [hep-ph].
 - [6] J. Aebischer, W. Altmannshofer, D. Guadagnoli, M. Reboud, P. Stangl and D. M. Straub, arXiv:1903.10434 [hep-ph].
 - [7] K. Kowalska, D. Kumar and E. M. Sessolo, arXiv:1903.10932 [hep-ph].
 - [8] M. Tanabashi *et al.* (Particle Data Group), Phys. Rev. D **98**, 030001 (2018).
 - [9] P. J. Fox, J. Liu, D. Tucker-Smith and N. Weiner, Phys. Rev. D **84**, 115006 (2011) doi:10.1103/PhysRevD.84.115006 [arXiv:1104.4127 [hep-ph]].
 - [10] C. Bobeth, A. J. Buras, A. Celis and M. Jung, JHEP **1704**, 079 (2017) doi:10.1007/JHEP04(2017)079 [arXiv:1609.04783 [hep-ph]].
 - [11] W. Altmannshofer, M. Carena and A. Crivellin, Phys. Rev. D **94**, no. 9, 095026 (2016) doi:10.1103/PhysRevD.94.095026 [arXiv:1604.08221 [hep-ph]].
 - [12] L. Darmé, K. Kowalska, L. Roszkowski and E. M. Sessolo, JHEP **1810**, 052 (2018) doi:10.1007/JHEP10(2018)052 [arXiv:1806.06036 [hep-ph]].
 - [13] D. Aristizabal Sierra, F. Staub and A. Vicente, Phys. Rev. D **92**, no. 1, 015001 (2015) doi:10.1103/PhysRevD.92.015001 [arXiv:1503.06077 [hep-ph]].